The Development of Optimal Charging Strategies for Lithium-Ion Batteries to Prevent the Onset of Lithium Plating at Low Ambient Temperatures

Upender Rao Koleti [1]*, Cheng Zhang[1], Romeo Malik[1], Truong Quang Dinh[1], James Marco[1]

[1] *WMG, The University of Warwick, Coventry CV4 7AL, United Kingdom*

Abstract

This study develops two novel charging strategies for lithium-ion batteries, designed to prevent the onset of lithium plating when the cells are charged at low ambient temperatures. Commercially available 3.1 Ah 18650-type cells with NCA and graphite electrodes have been selected for this study. Experimental results highlight that for these cells, lithium plating can be detected when the cells are charged with a traditional constant-current constant-voltage (CC-CV) profile at an ambient temperature of 5^{o}C and a charge rate of 1C. The occurrence of lithium plating is known to lead to a considerable capacity reduction. To avoid the onset of lithium plating with minimum impact on the charge time, two optimal charging strategies are proposed. The first is based on detecting the onset of lithium plating through the online analysis of the voltage relaxation profile (VRP). The second is to manage the cell charging process to achieve a pre-defined rate of battery degradation per charge cycle. Experimental results highlight that the capacity fade of cells using the proposed charging strategies can be significantly reduced compared to when charged using the conventional CC-CV approach by 45% and 70% respectively while minimizing their impact on the charging speed.

Keywords: Lithium Plating; Fast Charging; Lithium Ion; Voltage Relaxation Profile (VRP), Battery Management System (BMS)

Terms and Abbreviations

BMS	Battery Management System (BMS)
CC-CV	constant current followed by constant voltage
CC-CV-CC	constant current followed by constant voltage followed by constant current
DV	Differential voltage
EV	Electric Vehicle
LFP	Lithium Iron Phosphate
NCA	Lithium Nickel Cobalt Aluminium Oxide
NE	Negative electrode
NEP	Negative electrode potential
NMC	Nickel Manganese Cobalt Oxide
PDE	Partial Differential Equation
SEI	Solid Electrolyte Interface
SPM	Single particle model
SOH	State of Health
SOC	State of Charge
VRP	Voltage Relaxation Profile

* Upender Rao Koleti. Tel.:+44-7471114926; *E-mail address*: u.koleti@warwick.ac.uk.

1. Introduction

A number of recent studies, for example [1, 2] highlight the desire to rapidly charge lithium-ion batteries as one means of reinforcing consumer acceptance of the technology, particularly within mobile applications and the future electric vehicle (EV) market. However, research highlights that the use of "fast charging" (e.g. charge rates in excess of 1C), particularly at low ambient temperatures (less than 25^0C) will accelerate battery ageing [3, 4]. Lithium metal deposition on the graphite electrode will occur when the negative electrode potential (NEP) drops below the lithium reference potential. Lithium plating is defined within [5] as comprising of both reversible and irreversible elements. During the post-charge voltage relaxation period, described within [6], a portion of the plated lithium is reversed and intercalates within the electrode when the NEP rises above the reference value. The remainder, or irreversible plated lithium, may react with the electrolyte or become electrically disconnected from the electrode, thereby creating a pool of inactive metallic lithium [7]. While the irreversible component leads to a direct loss of the cyclable lithium, the reversible portion may indirectly reduce cell capacity further. The increased mechanical stresses within the electrode, because plated lithium occupies a larger volume than intercalated lithium [8], may over time cause a loss of active material due to mechanical deformation within the cell. In addition, the onset of lithium plating can negatively impact battery safety if dendrites are formed from isolated lithium metal. These dendrites may grow through the separator towards the cathode, resulting in an internal short circuit [9].

A number of studies have been reported within the literature that addresses the challenge of reducing lithium plating for lithium-ion batteries. These can be broadly categorized into model-based, intuition-based and experimentally based approaches. Model-based studies are typically underpinned by electrochemical models where the NEP is described by a set of partial differential equations (PDEs) based on the physical and electrochemical properties of the battery constituents such as the electrodes and electrolyte. Common model formulations include the P2D model [5], the single particle model (SPM) [10] and the single particle model with electrolyte (SPMe) [11]. By proper parameterisation, the models can be employed within the off-line simulation to quantify the NEP and therefore predict the onset of lithium plating for a given charge current. However, the use of such models within a real-time or online context is difficult because of the complexity of the governing equations and the need to parameterise such models. In addition, the magnitude of the potential drop at the negative electrode (NE) will vary as the cell ages, because of a number of degradation mechanisms such as electrolyte decomposition, active material cracking, loss of lithium and porosity reduction due to previously deposited lithium metal layers [12]. Also, the non-homogeneities within the cell construction such as different electrode particle sizes, their distribution and varying compression levels in the cell can lead to the onset of localized plating [13, 14]. These effects further compound the significant research challenge of extending these models to take account of the different degradation modes and to accurately represent the physical properties of the battery [15, 16].

As an alternative to the highly complex electrochemical model based current control, various intuitive current profiles are proposed within the literature to avoid the onset of lithium plating. These protocols include multistage constant current [17], pulsed charging current [18], temperature rise dependent charge current [19, 20], boost current [21], etc.

Although some of these intuitive charging profiles have shown improvements in extending battery life, a lack of theoretical guidance in the selection of charging current may not allow their optimization of the charging profile.

On the other hand, experimental approaches are based on destructive or non-destructive methods that aim to detect lithium plating or observe the NEP directly during battery charging. Destructive techniques are discussed within [22, 23] for irreversible plating detection. The studies present the use of Inductively Coupled Plasma Optical Emission Spectrometry (ICP-OES) analysis to an opened cell to identify lithium metal depositions [22]. While destructive plating detection techniques are able to provide definitive confirmation that non-reversible lithium plating has occurred, they are not suitable for real-time monitoring and charge-control applications.

Research presented within [9], highlights the use of modified cells for developing a plating mitigating charge profile. Thomas *et al*. use a destructive approach to observe the NEP and to devise a two-stage CC-CC (0.5C-0.2C) charge profile to maintain the NEP above the lithium reference voltage [9]. Here, the charge rate was maintained at 0.5C until the cell terminal voltage reached a level (defined as V_{tc}) at which the NEP was observed to reduce below the reference value. The applied charge rate in the second stage CC was then reduced to 0.2C as the charge continued. To monitor the NEP directly, the authors constructed a three-electrode cell with the harvested electrodes from a commercial cell. It is noteworthy that this modification may add a large number of uncertainties to the behaviour of the cell leading to difficulties in the repeatability and transferability of the identified V_{tc} value. First, the separation of electrodes from the commercial cell could increase the electrode impedance. Particularly, as discussed within [24], the process of clearing electrode material from one side of the current collector will modify physical electrode properties such as electrical conductivity and porosity. Secondly, the use of a different electrolyte within the cell will change the internal kinetics, and thus the potential drop within the cell. As shown in [9], the terminal voltage dynamics of the newly reconstructed cell were significantly different from those of the commercial (unmodified) derivative during the same high charge (1C) rate. Therefore, the results obtained from the reconstructed cell cannot be directly applied to the corresponding commercial cell. Further, this method cannot be used in many end-use applications because commercial cells do not have the third (lithium reference) electrode to monitor directly the electrode potentials, due in part because of the increase in cell weight and cost associated with the volume manufacture of such as device.

Recent studies highlight the use of non-destructive techniques to identify and quantify the reversible component of lithium plating. Existing studies [15, 25] indicate that the total amount of lithium plating is largely reversible in nature. One reason is that plating occurs on the negative electrode surface, which provides the required electrical contact between plated lithium and the electrode [15, 25]. Hence, reversible plating detection can be a reliable method of underpinning a future charge control strategy. Intercalation of the reversible part of the plated lithium into the NE changes the electrode lithiation level and potential which can be observed and used as an indicator of plating occurrence at the full cell level by monitoring the cell terminal voltage or by scanning the cell for the NE lithiation level. Reversible lithium plating detection can be performed using established techniques such as tomography [26], impedance spectroscopy [27], Differential voltage (DV) curves [15, 28] or Voltage Relaxation Profile (VRP) methods [26, 27]. Among these methods, VRP has the potential for deployment within real-time charge control

applications because it relies only on the cell terminal voltage as the basis for lithium plating detection and mitigation. Further, its application on different cell chemistries, such as NMC, NCA and LFP, highlights the potential transferability of the underpinning principles [26, 27].

To reduce lithium plating, a feasible solution is to (1) apply a high-rate CC charge until the cell terminal voltage has reached a pre-defined level (defined as $V_{HCC\text{-}end}$) lower than the full charge terminating voltage (V_f) and then, (2) reduce charge currents to reach the V_f. However, the selection of $V_{HCC\text{-}end}$ is critical since the use of a lower value for $V_{HCC\text{-}end}$ compared to V_{tc} prolongs the charging time unnecessarily, and a higher value fails to avoid lithium plating completely. Therefore, for the proper selection of $V_{HCC\text{-}end}$, it is necessary to identify V_{tc} through a destructive approach or to optimise $V_{HCC\text{-}end}$ to reach un-known V_{tc} using a non-destructive approach.

In this paper, the authors propose two novel non-destructive strategies to identify the V_{tc}, and thus the onset of lithium plating by optimising the $V_{HCC\text{-}end}$. The first approach is underpinned by the use of the VRP technique in which the occurrence of lithium plating is monitored after every charge cycle to regulate the $V_{HCC\text{-}end}$ in such a way that it approaches the unknown V_{tc} where lithium plating begins to occur. The resulting $V_{HCC\text{-}end}$ is then used for cell optimal charging. Unlike the previously proposed plating control techniques [9], this method is directly based on experimental lithium plating detection without the need for cell dismantling. For the second approach, the V_{tc} is identified using a measure of overall capacity reduction per cycle to optimise the charging time for the battery and to extend its operational life. These approaches based on onboard measurable parameters and their measurable rate of change are consequently useful for fast charging control applications. For both charge control strategies, experimental results are presented that clearly show their ability to minimise battery degradation without compromising battery charge time significantly. To facilitate comparison, results are presented for cells charged with the traditional CC-CV approach.

This paper is structured as follows. The research methodology associated with the development of modified charge control strategies underpinned by lithium plating detection and the capacity fade rate is presented in Section 2. In Section 3, the experimental plan and experimental setup are introduced. Section 4 presents the experimental results that demonstrate the effectiveness of the new charge profiles when compared to conventional battery charge methods. Conclusions from this research provided in Section 5.

2. Development of Charging Control Strategies

2.1 A Conventional Charging Strategy

The constant current followed by constant voltage (CC-CV) charge protocol is widely employed in many battery applications because of its simplicity [2]. Reduced charging times can be achieved by the use of higher currents in the CC phase, which as discussed in Section 1, can lead to lithium deposition when charging the battery at higher States of Charge (SOC) and therefore faster ageing [9]. It is well understood, that the SOC level at which lithium plating commences depends on a number of factors that include: ambient temperature, charge current and cell type [9, 29]. Figure 1a shows an example of the CC-CV charge profile along with the NEP. At the end of the 3A (charge rate of 1C) CC phase, the cell voltage has risen to 4.2V. The CV phase maintains the cell voltage until the charge current has reduced to 0.75A (charge rate of 0.25C). The NEP reaches its lowest value at the end of the CC phase [9, 21]. As it falls below the

Li reference potential, lithium plating may occur. To avoid lithium plating, a lower charge current in the CC phase may be employed. However, for significant reductions in charge current, this increases the charge time considerably. For example, reducing the CC phase charge rate from 1C to 0.5C would increase the charge time from 1.7 hours to in excess of 2.6 hours [2].

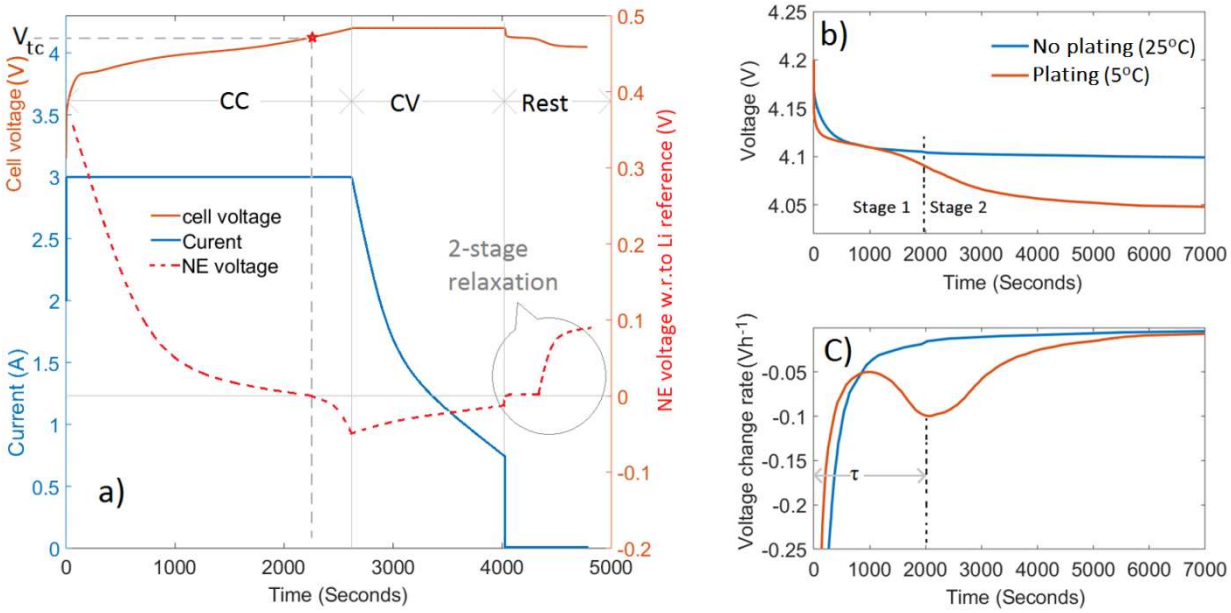

Figure 1: a) CC-CV charge profile: Current, cell voltage measurements and illustrative negative electrode potential; b) Cell voltage relaxation behaviour with and without lithium plating and C) their differential

2.2 Reversible Plating Detection using VRP Method

A full description of the VRP method; its derivation, application and underpinning theory is discussed in [26, 30] and will therefore not be repeated here. For completeness, a brief introduction is provided. This method is based on how the cell terminal voltage is influenced by the lithium plating reverse reactions. In the post-charge region, shown in Figure 1a, the NEP starts to recover between time 4000 and 5000 seconds. Once the NEP exceeds the reference value, intercalation of the reversible portion of plated lithium into graphite will commence [31]. During the time that plating reverse reactions occur, the NEP will remain constant. The voltage relaxation observed at the battery terminals continues after the completion of lithium stripping. As shown in Figure 1a, this reaction manifests as a change to the single stage relaxation profile within the cell terminal voltage, in which a two-stage voltage relaxation can be observed (e.g. between a time of 4000-5000 seconds). This unique feature of the cell terminal voltage during the rest period after charging is used to infer the occurrence of the reversible part of lithium plating [26, 27]. Figure 1b demonstrates the difference in cell terminal voltage relaxation between a non-plating condition (single stage profile) and a charge event in which lithium plating has occurred (two-stage profile) [26, 27, 31]. The differential of the cell voltage (shown in Figure 1c) can be utilised to identify the time to complete the reverse reactions (often called the “stripping period” and defined as τ in Figure 1c). This stripping period can be used as a relative measure to quantify the amount of reversible lithium plating that occurred in the proceeding charge event. The study in [26] indicates that the stripping period found from the VRP method is directly proportional to the amount of reversible plated lithium.

2.3. Proposed Charging Control Strategies

In this work, a three-stage (CC-CV-CC) charge protocol is derived to reduce the onset of lithium plating and therefore plating induced battery degradation while concurrently minimizing the charge profile impact on the charging time. Two methods are introduced that both employ the same three-stage, CC-CV-CC, charge profile. The primary difference between their implementation is the method used to regulate and optimize the $V_{HCC\text{-}end}$. Detection of lithium plating and thus regulation of $V_{HCC\text{-}end}$ is achieved using either a measure of τ derived from the VRP method (discussed in Section 2.3.2) or from a direct estimate of capacity reduction per charge cycle defined as ΔSOH/cycle (discussed further in Section 2.3.3). Where the state of health (SOH) is defined as the ratio of the measured capacity vs the nominal value when the cell was new.

Figure 2 shows a generalised block diagram representation for the proposed charge control strategy online implementation that would underpin its application within a BMS. Since a standard BMS monitors the cell voltage and tracks the SOH changes, both these approaches can be incorporated into the BMS that updates the charger with the latest $V_{HCC-end}$ for the next charge event. Development and Implementation of both the charge profiles are detailed in the sections 2.3.2 and 2.3.3.

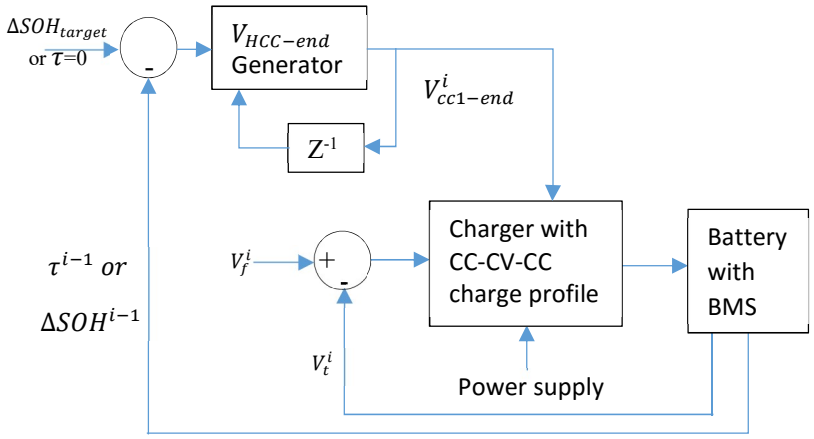

Figure 2: Online charging control proposition

2.3.1 CC-CV-CC Charge Profile Development

Figure *3* presents a comparison of the proposed CC-CV-CC protocol with the conventional CC-CV charge profile. In the CC-CV-CC profile, the first CC phase is applied until the cell voltage reaches V_{tc}. In this study, 1C charge rate is employed in the first CC stage. The CV phase is applied once the terminal voltage equals V_{tc} avoiding the NEP reducing below the reference value and therefore the onset of plating [9]. This is in contrast to the traditional CC-CV process in which the CC phase is maintained until 4.2V and the NEP reduces below the reference value at a time of 1800 seconds. The CV phase is maintained until the value of charge rate falls to 0.25C. To avoid lithium plating and to improve charge time, charge current in the third stage must be appropriately selected. From [30], for this cell, it was found that lithium plating was not detected with charge rates lower than 0.25C at ambient temperatures above 5°C and reversible plating detection ability was maximum with a cut-off charge rate of 0.25C. As discussed in [30], lithium stripping begins in the

CV phase itself if the CV cut-off charge rate is below 0.25C that reduce the stripping lithium amount in the rest period and thus, detection ability of reversible plating using the VRP method comes down. Therefore, the CV phase is maintained until the charge rate reduces to 0.25C and then the constant 0.25C charge rate is maintained until the cell voltage measures 4.2V. Hence, the proposed charge profile becomes 1C-CV-0.25C as shown in

Figure *3*. It is noteworthy, that as discussed within [32], the value of V_{tc} will vary as the cell ages and other degradation mechanisms impact the overall capacity and impedance of the cell. As a result, the value of V_{tc} must be re-evaluated during the operational life of the battery.

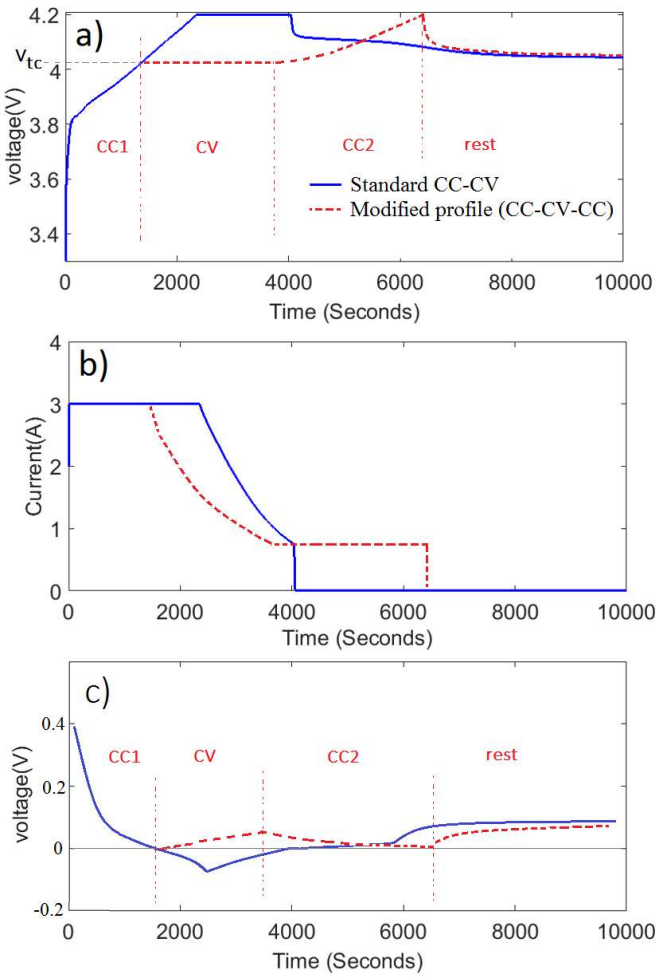

Figure 3: Proposed 3-stage and the conventional CC-CV charge protocol: a) cell voltage b) charge current and c) illustrative negative electrode potential

2.3.2. Plating Detection-Based Charging Control Strategy

To identify the correct value of $V_{tc,}$ the VRP method is employed to detect the occurrence of reversible lithium plating within the proceeding charge event. Within the context of this experiment, V_{tc} is assumed to be unknown at the start. As a result, the CV phase voltage or the high rate first stage CC terminating voltage ($V_{HCC\text{-}end}$) can commence from a fixed value during the first cycle. In this study, $V_{HCC\text{-}end}$ for the first cycle is set to be 4.2V. If lithium plating is detected after the first battery charge event it implies that that value of $V_{HCC\text{-}end}$ is greater than $V_{tc.}$ The value of $V_{HCC\text{-}end}$ is therefore reduced by an amount equal to ΔV for the next charge event. Conversely, in the case when lithium plating is not

detected, $V_{HCC\text{-}end}$ can be increased by ΔV for the next charge cycle (while maintaining the upper and lower limits for cell voltage defined by the manufacturer). This adjustment to $V_{HCC\text{-}end}$ continues at the end of each fast charge event until $V_{HCC\text{-}end}$ reaches the target value V_{tc} as depicted in Figure 4a. The selection of the voltage step size (ΔV) is detailed in the next section.

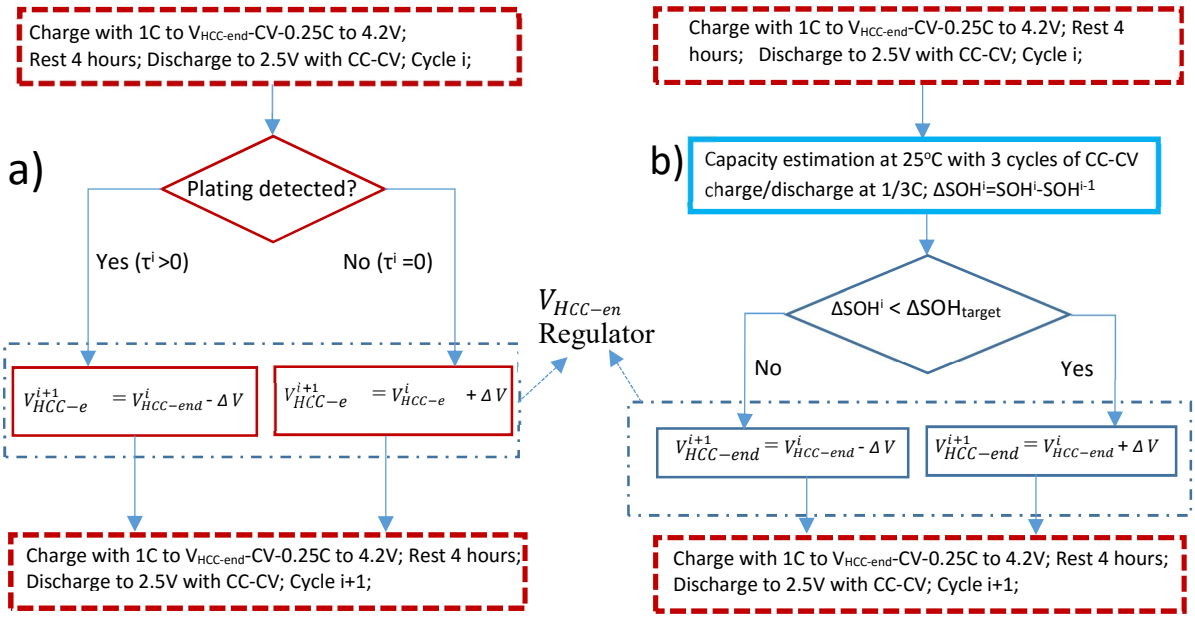

Figure 4: Flowchart for charging control using a) plating detection and b) ΔSOH

2.3.3 Capacity Fade Rate-Based Charge Control Strategy

In this technique, the value of $V_{HCC\text{-}end}$ is determined using the estimated capacity reduction per charge cycle to minimise battery degradation. It is noteworthy that this technique employs overall capacity fade as the control variable and therefore considers other battery degradation mechanisms that may occur, such as solid electrolyte interface (SEI) formation, when the cell is under charge. To facilitate capacity fade rate-based charge control, the target value of capacity reduction per cycle, defined as ΔSOH_{target} needs to be defined. Obviously, the lower the ΔSOH_{target} is set, then conceptually the longer the battery life, but with the implication that charge times will become excessive. Generally, when lithium-ion cells are continually cycled at low charge/discharge rates (e.g. less than 0.25C) and ambient temperature, after the initial few cycles, the battery will exhibit an almost linear capacity fade [29] for much of its operational life. The ΔSOH_{target} can be defined based on this linear capacity fade rate. The ΔSOH_{target} in this work is selected based on the author's previous low-temperature battery cycling results, reported within [30]. This research reported that the cells lost circa 10% capacity in ten cycles at 5°C and 1C charge/discharge rate with the CC-CV charging protocol [30]. This equates to a 1% ΔSOH per complete charge cycle. Therefore, by setting ΔSOH equal to 0.1%, the assumption is made that this would, in principle, extend the life of the cell by a factor of 10. On this basis, if the ΔSOH/cycle in the current cycle is higher than ΔSOH_{target}, $V_{HCC\text{-}end}$ is decreased by ΔV for the next cycle as depicted in Figure 4b. In this approach, an accurate estimate of ΔSOH and therefore cell capacity measurement is necessary. To measure a ΔSOH/cycle value of 0.1% with a relative error of ± 5%, the current measurement accuracy must be in the order of ± 0.005%. An alternative approach is not to calculate ΔSOH after each charging event. For example, if the capacity is measured once in five charge cycles, a 0.5% ΔSOH change can be measured using a ± 0.025% accurate current

sensor. This yields an average ΔSOH/cycle between 0.095 and 0.105% which meets the target requirement of 0.005% accuracy. However, the consequence of this hardware limitation is that $V_{HCC\text{-}end}$ is regulated only once in five cycles instead of cycle-by-cycle and therefore the cell may be subject to extended periods of degradation.

3. Experimental Design

3.1 Cell Selection and Test Case Definition

Commercially available lithium NCA-based 18650 cells were used to study the onset of lithium plating under the different charge methods defined in Section 2. For this cell, the negative electrode is made from Graphite. The cells have a rated capacity of 3.1 Ah between 2.5 V and 4.2V at an ambient temperature of 25^0C and a discharge rate of 1/3C. Three cells for each charge method (CC-CV; CC-CV-CC VRP based charge control and CC-CV-CC ΔSOH based charge control) were used. As shown in Table 1, 9 cells were therefore employed during the experimentation to minimise the effects of cell-to-cell variations on the experimental results. For ease of reporting, the cells were classified as being within one of three groups: A, B or C with individual cell markings, for example, C_{A1}, C_{A2}, C_{A3} respectively for the three cells within Group A.

Table 1: Test cases and cell requirements

Charge protocol	Cells used (group: cell marking)
Conventional CC-CV	Three new cells (A: C_{A1}, C_{A2}, C_{A3})
VRP based charging control	Three new cells (B: C_{B1}, C_{B2}, C_{B3})
ΔSOH based charging control	Three new cells (C: C_{C1}, C_{C2}, C_{C3})

3.2 Experimental setup

All experiments were performed inside a thermal chamber (Model: ESPEC PL-3KPH), with the cells electrically loaded using a Maccor cell cycler (Model: Series 4000). The Maccor unit enables the measurement of the cell voltage and current with an accuracy of ± 1 mV and ± 0.03 mA respectively. In addition, K-type thermocouples with an accuracy of ± 1.5°C were attached to the negative tab of each cell to measure the cell surface temperature. The test parameters are summarised in Table 2.

Table 2: Measurement parameters and their range and accuracies

Measuring parameter	Measurement range	accuracy	Resolution	Sampling time
Voltage	2.5 to 4.2V	+/- 1 mV	0.1 mV	0.1 second
Current	+3 to -3A	+/- 0.02%	0.030 mA	0.1 second
Temperature	0 to 30°C	+/- 1.5°C	0.01°C	1 second

As discussed within [33], during continual charge-discharge experiments the cell temperature may rise, even when installed within a thermal chamber due to internal heat generation and subtle variations of temperature within the chamber volume. Varying charge profiles and different ageing levels within the cells can lead to larger variations in cell temperature between the samples. This makes the comparison of reversible plating difficult since the lithium reversing reaction rate rises with increasing temperature [28]. Cells were therefore installed within a manifold and liquid

surface cooling used to maintain cell temperature at the desired value using a LAUDA controller (Model: Proline RP 845 C) with the ability to regulate temperature to an accuracy of ± 0.1°C. As observed in this work, irrespective of the operating conditions, the surface temperature of these cells were maintained at the set temperature within ±0.5 °C with the active cooling mechanism.

3.3 Experimental Procedure

Figure 5 presents the procedure for cell experiments using the three different charge control strategies. The experiments comprised of three stages, defined as:

- Cell Pre-Conditioning,
- Fast Charge tests, and
- Capacity Characterization

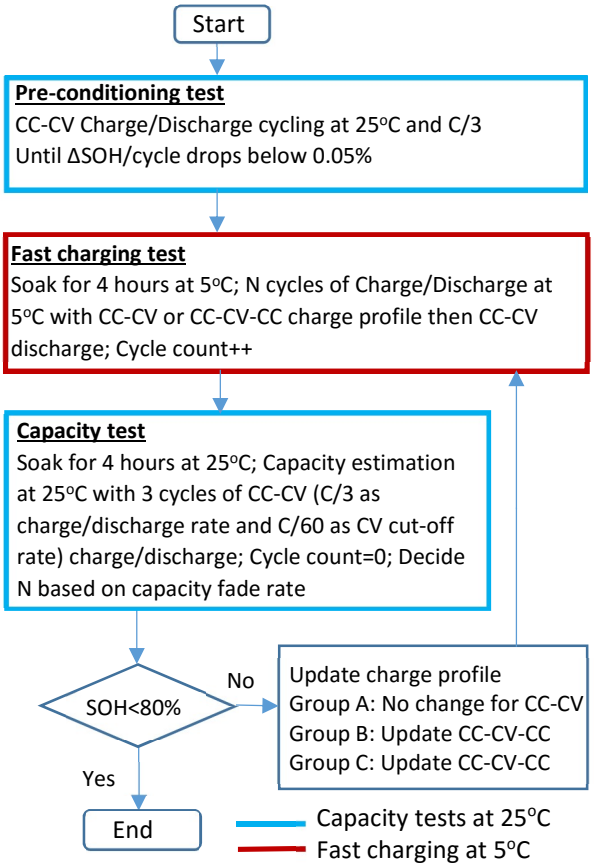

Figure 5: Procedure for experiments with cell charging

3.3.1 Cell Pre-Conditioning Tests

Side reactions between the electrolyte and electrode surface are known to form an SEI layer over the negative electrode [34] which leads to cell capacity reduction. These side reactions reduce within the first few cycles as the SEI thickness increases. Consequently, this slows the growth rate of the SEI layer and thus the capacity reduction within the cell. To minimise the contribution of the SEI layer growth to the ΔSOH/cycle estimation, all nine cells irrespective of their charge protocol were cycled at 25°C with CC-CV (CC charge/discharge rate of 1/3C and CV cut-off charge/discharge rate of

C/60) until the rate of ΔSOH/cycle was less than 0.05%. The CV during discharge in both preconditioning and capacity estimation tests was included in this work to alleviate the impact of impedance on the measured capacity of the cell. The kinetics of lithium exchange between the electrodes, and thus the impedance to the current flow in the battery varies according to the electrode's inhomogeneities [35], deactivation of electrode particles due to porosity reduction [12], anode overhang [36, 37] and battery degradation level [38]. As discussed within [35], using a CV discharge with a sufficiently low cut-off current can reduce the impedance effect on the battery capacity estimation. Once the pre-conditioning tests were completed, the cells were then deemed ready for fast charge experiments and further capacity characterisation.

3.3.2 Fast charging cycle tests

To provoke lithium plating and to enable its control, the cells were cycled at low temperature with high charge currents. The cells were allowed to soak for 4 hours at a temperature of 5°C before performing the fast charging tests to ensure that they had reached equilibrium. For all cells, a high charging current of 3A (1C rate) was applied in the first CC phase and the charge was terminated when the cell voltage reached 4.2V with 0.75A (0.25C) current in the final stage. However, the current profile between these two values was varied based on the charge control strategy adopted.

- For the traditional CC-CV charge protocol; the 1C charge rate was applied until the cell voltage reached 4.2V and then the CV phase was maintained at 4.2V until the charge rate reduced to 0.25C.
- For the ΔSOH charge protocol; the 1C charge rate was applied during the first stage CC phase until the cell voltage reached $V_{HCC\text{-}end.}$ CV charging was then maintained until the charge rate dropped to 0.25C. The 0.25C value was maintained until the cell voltage reached 4.2 V. Identification of $V_{HCC\text{-}end}$ was based on the method defined in Section 2.3.3.
- For the Plating Detection Charge Protocol; the same 1C charge rate was applied during the first stage CC phase until the cell voltage reached $V_{HCC\text{-}end.}$ CV charging was again maintained until the charge rate dropped to 0.25C. The 0.25C value was maintained until the cell voltage reached 4.2 V. However, the identification of $V_{HCC\text{-}end}$ was based on the VRP method described in Section 2.3.2.

For all conditions, once charging had ceased (cell voltage equal to 4.2 V with a 0.25C/h charge current), a rest period of 4 hours was allowed to monitor cell voltage and temperature and to allow the cells to equilibrate. After 4 hours, the cells were discharged to 2.5V with CC-CV (using a CC discharge rate of C/3 and a CV cut-off discharge rate of C/20) to complete one fast charge cycle.

3.3.3 Capacity characterization tests

To support derivation of the ΔSOH cycle-based charge profile development, the fast charging profiles were interrupted and the temperature of the cells raised to 25 °C and left to rest for 4 hours. The number of fast charge cycles (defined as N) between capacity tests was varied according to the measured rate of capacity fade. Adjustment of N helps in two ways. Firstly, a low value of N when the capacity fade rate is deemed to be high (e.g. greater than 0.5%) permits a faster intervention in the charge profile to reduce the magnitude of battery degradation. Secondly, a higher value for N when

the capacity fade rate is slow (e.g. less than 0.1%) reduces the overall test period. From [30], it was found that the rate of capacity reduction was comparatively high during the early cycles and then slowed as the level of battery degradation increased. Hence, for the first 4 fast-charging cycles, the capacity test was performed after each fast charge cycle (N=1). The capacity assessment was then undertaken every 3 cycles (from 5th to 13th fast charge cycles) and after 6 fast-charge cycles, from that point onwards. Table 3 summarises the frequency variation of capacity tests with cycle number during the ΔSOH cycle-based charge profile development.

Table 3: capacity test interruption to the fast charging cycles

The fast Charging cycle number	Capacity test frequency
1 to 4	After every fast charging cycle
5 to 13	Once per 3 fast charging cycles
14 to 52	Once per 6 fast charging cycles

To facilitate comparison, all capacity tests used a CC-CV profile with C/3 charge/discharge rate in the CC phase and a cut-off charge/discharge rate of C/60 in the CV phase at 4.2V and 2.5 V for both charge and discharge respectively. Further, all the cells were tested for capacity at same intervals of fast charging cycles for a better comparison of results since the capacity estimation procedure that interrupts the ageing tests has a significant influence on the battery life [39].

In the capacity test, when the capacity retention level measured was found to be greater than 80% of the initial capacity for all cells, the cells were subject to a further round of fast-charging as shown in Figure 5. While the fast charge profile was unaltered for the cells loaded with the traditional CC-CV protocol, $V_{HCC\text{-}end}$ values were updated for the cells from sets B and C (from Table 1). As discussed, for the cells with from set B, the charge profile was updated based on the level of lithium plating detected in the last fast charging cycle. Here, the step change (ΔV) was set to 100mV in the initial cycles until lithium plating was detected and then it was reduced by 25mV to further fine tune the desired value of $V_{HCC\text{-}end}$. For cells from Set C, the charge profile was updated based on the capacity tests at 25^{o}C and the ΔV value used in the study was initially set to 50mV until the ΔSOH/cycle reached the ΔSOH_{target} of 0.1% and then it was reduced to 25mV to further fine tune the transition point between the CC-CV phase of battery charging.

4. Experimental Results & Discussion

4.1 Results

4.1.1 Conditioning Tests

The conditioning tests were undertaken at ambient temperature to reduce the impact of the SEI layer growth rate on the fast charging experimental results. The results show that the discharge capacity was lower than the charge capacity in every cycle. By the sixth cycle, the magnitude of capacity change per cycle and the capacity difference between charge and discharge had reduced, indicating that the cells were asymptotically stable in terms of capacity retention with less than 0.03% change in capacity reduction per cycle. The value of cell capacity measured at the cycle 6th was taken as the cell initial capacity prior to the fast-charge cycles. For completeness, Table 4 presents the actual values of capacity measured for each cell at the end of the 6th conditioning cycle.

Table 4: Measured nominal capacity values for each cell under test, after 6 conditioning cycles

Cell Identifier	Capacity after 6th Conditioning cycle (Ah)
C_{A1}, C_{A2}, C_{A2}	3.151, 3.171, 3.167
C_{B1}, C_{B2}, C_{B2}	3.182, 3.169, 3.172
C_{C1}, C_{C2}, C_{C3},	3.174, 3.191, 3.168

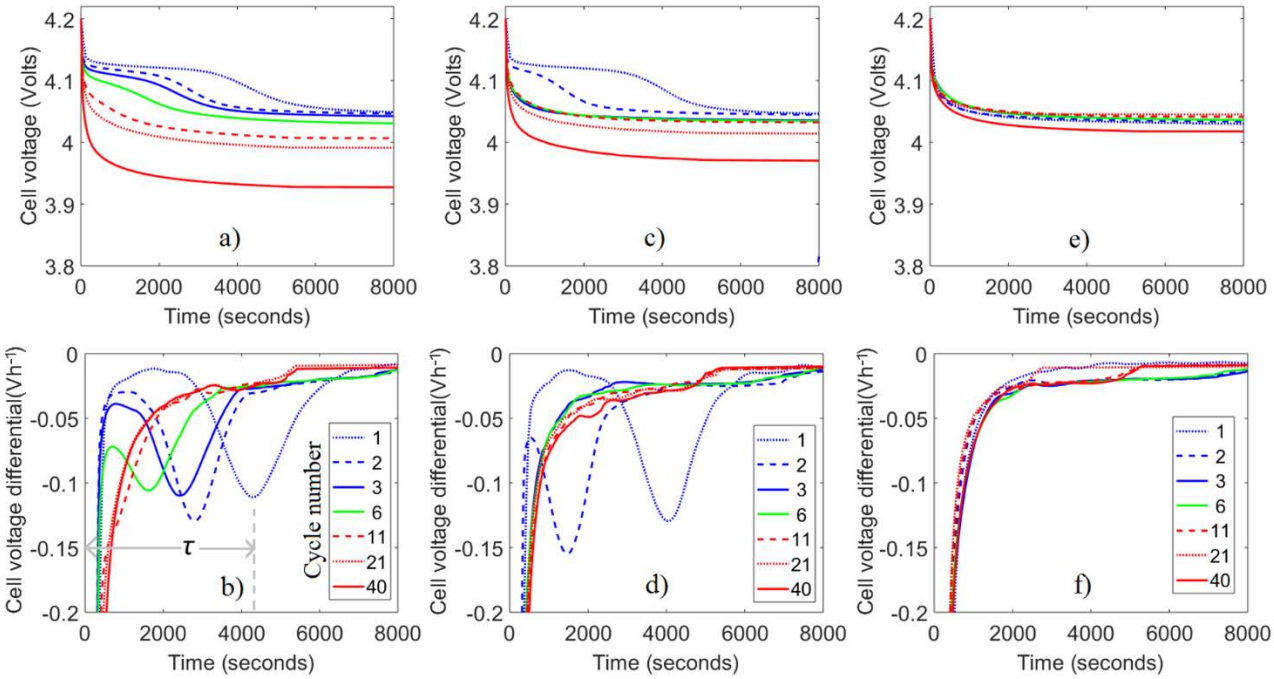

Figure 6: Reversible plating detection using cell voltage relaxation in rest period - Cells under CC-CV protocol a) cell voltage and b) its differential; Cells using plating detection-based charging protocol changing c) cell voltage and d) its differential; Cells using ΔSOH based charging protocol e) cell voltage and f) its differential at different fast charging cycles

4.1.2 Traditional CC-CV Charging Control

Set A cells were operated under the traditional CC-CV charge profile until they lost an average of 20% of their nominal capacity. In addition to capacity fade and charging time trends, these cells were also monitored for lithium plating occurrence using the VRP method with the help of a 4 hour rest period at the end of every fast charge event. Figure 6a and Figure 6b present the post-charge voltage relation profiles and their differential respectively at different fast charging cycles. The onset of Lithium plating can be observed and reversible plating decreasing with increasing cycle number. In the first cycle, the stripping period was found to be circa 4300 seconds, which reduced to 2800 seconds in the next charge cycle. Since, as discussed within [26], the stripping period is deemed to be in proportion to the amount of reversible plating, it can be assumed that reversible plating detection levels are equally reducing with cycle number. One possible reason is a loss of active lithium because of lithium plating can reduce the NE lithiation levels towards the end of charge, and thus

decreases lithium plating amounts with the increasing cycle number [15]. With further progress of fast charging cycles, no reversible plating was detected after the 11th fast charge cycle. To confirm the plating detection using the VRP method, one cell from Set A and one new cell for comparison were opened in an argon-filled glove box and the graphite electrodes were inspected visually for metallic depositions following a method described within [22]. The graphite electrode of the new cell appears black as shown in Figure 7a, as is expected from a functional fully discharged graphite-based electrode. Conversely, clearly visible areas at the axial edges of cell A were covered by silver colour depositions as shown in Figure 7b. As discussed within [22], since the graphite electrode does not appear in silver colour at any of its lithiation levels, these depositions can be attributed to lithium plating. Therefore, cell A was exhibiting lithium metal depositions, which is in line with the lithium plating detection using the VRP method.

Figure 7: Photographs of graphite electrodes: a) new cell and b) Set A cell

4.1.3 Plating Detection-Based Charging Control

Similar to set A, in the first cycle where $V_{HCC\text{-}end}$ was predefined to 4.2V, significant levels of lithium plating were observed using the VRP method in the cells contained within set B. Figure 6c and Figure 6d show the cell voltage and its differential respectively in the post-charge 4 hour rest period. By employing the charge control method, $V_{HCC\text{-}end}$ was reduced to 4.1V in the second cycle to reduce the level of plating occurring. Accordingly, the observed stripping period was reduced to 1250 seconds from 4100 seconds. Since lithium plating was still observed in this cycle, $V_{HCC\text{-}end}$ was further reduced by another 100mV to 4.0 V for the third fast charge cycle. In the third cycle, no reversible plating was detected, indicating that V_{tc} was between 4.0 and 4.1V. To further refine the estimate of the critical voltage where the NEP reduces below the reference value, $V_{HCC\text{-}end}$ was increased over the next fast-charge cycles in steps of 25mV until the lithium plating was again detected. However, for these results plating was not identified in any subsequent fast charge cycle. This resulted in the rise of $V_{HCC\text{-}end}$ back to 4.2V. The drop in reversible plating detection levels with cycle number indicates that the reversible plating was either reducing or becoming too difficult to detect using the VRP method. The possible reasons for the detection failure using the VRP approach are further discussed in Section 4.2.3.

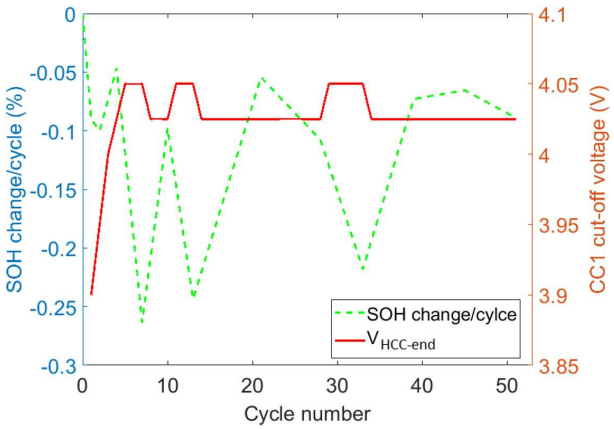

Figure 8: First stage CC end voltage and capacity fade with the cycle number for the ΔSOH based charge profile

4.1.4 ΔSOH Based Charging Control

The CC-CV-CC charge protocol was applied for the ΔSOH-based charging control with the $V_{HCC\text{-}end}$ initially set to 3.9V in the first cycle. Since the first four cycles were found with ΔSOH/cycle values lower than 0.1%, $V_{HCC\text{-}end}$ was increased in four steps from 3.9 V in the first cycle to 4.025 V in the fourth cycle as shown in Figure 8. A further increase of $V_{HCC\text{-}end}$ to 4.05 V in the next three cycles (cycle 5, 6, 7) resulted in a rise of ΔSOH/cycle to circa 0.25%. To reduce the capacity reduction per cycle, $V_{HCC\text{-}end}$ was subsequently decreased to 4.025 V for the eighth cycle. This reduced the ΔSOH/cycle level to below the ΔSOH_{target} (0.1%). From this point, any rise of $V_{HCC\text{-}end}$ from 4.025 to 4.05 V consistently resulted in a ΔSOH/cycle value above the threshold of 0.1%. Figure 8 shows the variation of $V_{HCC\text{-}end}$ and capacity fade rate with cycle number. A $V_{HCC\text{-}end}$ value of 4.025 was seen as the optimum value to maintain the ΔSOH/cycle lower than 0.1%. The result also shows that reversible lithium plating was not observed (as per Figure 6e and Figure 6f) for the cells under this charging control strategy during any fast charge cycle. One reason for this may be because of the lower initial starting voltage of 3.9V that was employed to transition the charging profile between the CC-CV phases.

4.1.5 Comparison of Results between the Three Charging Profiles

Figure 9 compares the performance of the cell sets (A, B and C) for the different fast charge strategies. The discussion is focussed on the rate of capacity reduction due to fast charging each cell, the value of $V_{HCC\text{-}end}$ and the corresponding charge time.

Capacity Fade Analysis

From Figure 8a it can be seen that battery life could be extended by employing the proposed fast charge control techniques. By using the plating detection-based method, the cells lost an average of 11% capacity compared to an average of 20% reduction for cells using the traditional CC-CV protocol. The reason for the large capacity reduction for the CC-CV charge protocol was the existence of lithium plating observed in the first ten cycles (see Figure 6b) and potential secondary effects of lithium plating in the form of SEI growth and porosity changes in the electrode [12]. This is in contrast to the cells charged using the CC-CV-CC profile with the transition between the CC and CV phase governed by the plating detection-based control. The results show that reversible lithium plating was only found in the first two

fast charge cycles. This reaffirms the findings from [30] and the literature contained within [3, 22] that higher levels of plating lead to increased levels of capacity reduction and therefore must be avoided to prolong battery life.

With the ΔSOH-based charge strategy, the level of capacity reduction was further reduced for cells from set C, when compared to set A and B. The cells with the ΔSOH-based control lost only an average of 6% capacity after 52 cycles, compared to an average of 11% capacity reduction from cells from set B. The reason for this was the maximum operated voltage in the ΔSOH-based control, $V_{HCC\text{-}end}$, was only 4.05 V. Low values of $V_{HCC\text{-}end}$ can benefit the cell in two ways. First, terminating the high CC stage at a lower cell voltage level can reduce or avoid lithium plating since the probability of occurrence of lithium-plating is higher at higher SOC or at higher cell voltage levels [1, 9]. The experimental results show that reversible plating was not observed for the cells using the ΔSOH-based control method, which means that either lithium plating was completely avoided or reversible plating was below the detectable level using this technique. In addition, it can be hypothesised that the low level of $V_{HCC\text{-}end}$ voltage below 4.05 V could reduce other ageing mechanisms such as SEI growth or cycle induced mechanical stresses within the cell. Section 5 discusses these factors further within the context of overall battery degradation.

Cells observed with lithium plating in the early cycles continued to lose higher levels of capacity in the later cycles where plating was not detected. For the cells from set A charged using the CC-CV profile, lithium plating was observed to occur until the fast charge cycle number 10 (Figure 6b). During the next 42 cycles, these cells lost 11% capacity where lithium plating was not detected (Figure 9a), that equates to an average capacity loss per cycle of 0.162%. Similar results were observed for the cells from set B that used the plating detection control method. For this case, lithium plating was observed after the first 2 cycles (Figure 6d). The cells proceeded to lose 9.2% capacity in the next 50 cycles where plating was not detected (Figure 9a), i.e. 0.184% loss per cycle. Conversely, lithium plating was never observed for the cells from set C that employed the ΔSOH control technique. For these cells only a 5.9% capacity reduction throughout the 52-cycles of fast charging (Figure 9a), i.e. 0.113% per cycle was experienced. This implies that the previous exposure to lithium plating for the cells may have a long-term negative impact on battery life and therefore cell SOH. As discussed in section 4.2.3, there are several possible reasons for this that include: 1) the deposited lithium metals from the previous plating events may cause further battery degradation; or 2) the ability to detect lithium plating may be reducing with ongoing battery degradation, which fails to detect the occurrence of plating.

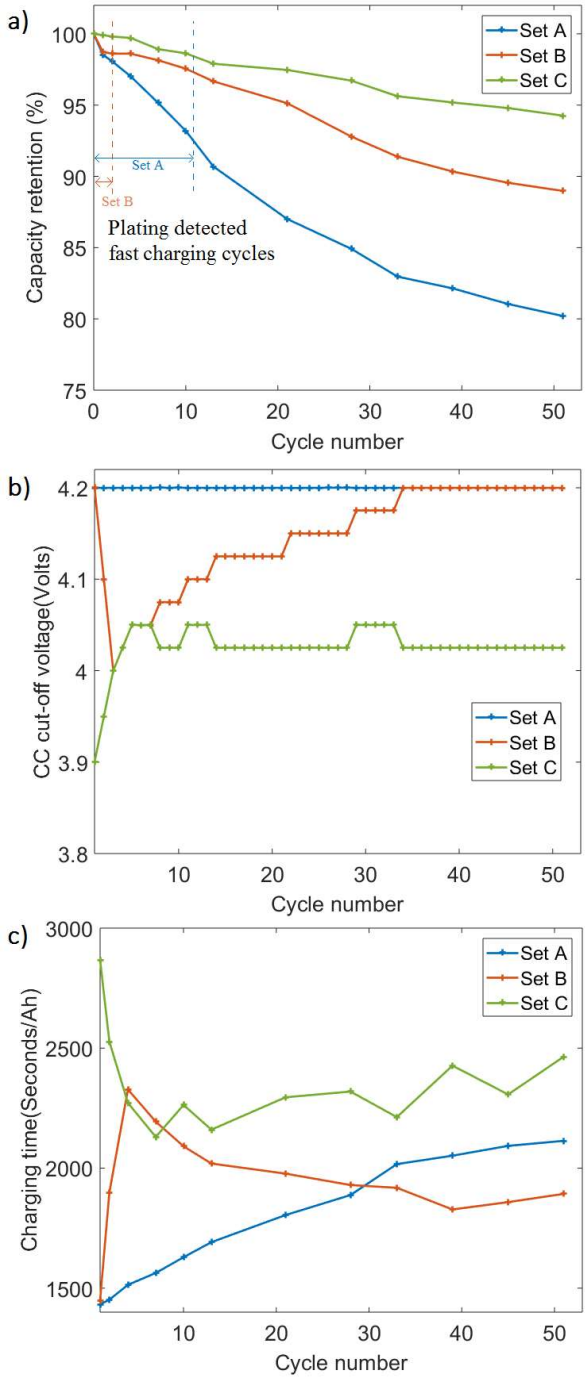

Figure 9: Comparison of the average cell performance using different charging control strategies: a) Charge retention, b) first stage CC end voltage value and c) charge time as a function of cycle number

Charge Time Analysis

From Figure 9c, the cell charging time was normalised for improved ease of comparison. The normalized charging time was defined as the charging time per ampere-hour (time/Ah). From Figure 8c, the following observations can be made:

- The value of charging time is highly dependent on the duration of the first stage CC phase during fast charging when the charging current is high. Figure 9c shows the charging time variations over each cycle of the three charge profiles. For newer cells, the higher the $V_{HCC\text{-}end}$ threshold is, the longer the duration of the first stage CC phase is.

As a result, the charging time overall was lower. For example, to charge one Ah capacity, the cells in set A ($V_{HCC\text{-}end}$ = 4.2V) took only 1420 seconds while the cells in set C ($V_{HCC\text{-}end}$ = 3.9V) took 2860 seconds, an increase of just over 100%.

- The impact of $V_{HCC\text{-}end}$ on the overall charge time could reduce with the value of capacity reduction. As seen in Figure 9c, the charging time for cells from set C, using ΔSOH based control protocol was 100% higher than the CC-CV protocol at the start of experimentation. This was improved to a value circa 20% higher than the CC-CV protocol towards the end of experimentation.
- More noticeably, it was found that plating-based charge control (set B cells) experienced an improvement in both charging time and battery life when compared to cells charged with the traditional CC-CV profile. Figure 8c shows that the value of charge time varied from 50% higher after the fifth cycle to 15% lower for the 50th cycle. The key crossover point was the 30th fast-charge cycle. This observation is highly significant because it implies that over time, the modified charging approach simultaneously yields reduced battery charge times and extends battery life. The reason for this is that the increased impedance associated with battery degradation reduces the CC phase charge time because of the increased potential drop. As a result, the charging speed of the CC-CV profile with highest levels of degradation was significantly reduced in the end and the charging time difference between the CC-CV and proposed new charge profiles was reduced.

4.2 Discussion of Results

4.2.1 Large Reversible Plating Levels

As shown in [26], the minimum threshold for reversible plating detection for the selected cell at 0^{o}C was around 2.5% of the nominal capacity using the VRP method. According to the authors, observable features from the cell terminal voltage are not identifiable when the reversible plating levels are lower than 2.5% [26]. This threshold level can increase with increasing ambient temperature because of the reverse reactions rate rise or the stripping time may reduce [28]. From Section 4.1, in the first cycle of set A test results, reversible plating was observed with a stripping period of circa 4300 seconds (Figure 6). The minimum stripping period identified from the results was about 800 seconds that was found after the 10th cycle.

If an assumption is made that the 800 seconds stripping time corresponds to a reversible plating level at 2.5% of the charged capacity, as identified within [15], then the 4300 second stripping time found for the first cycle implies that circa 13.4% of the charged capacity could form part of the reversible plated lithium. From the experimental results shown in Figure 9a, the cells lost about 1.5% capacity after the first cycle. This further implies that irreversible plating was no more than 1.5% of the charged capacity. Therefore, the ratio between reversible and irreversible plating may be estimated as being 13.4%:1.5% or 8.96:1. This simplified analysis reinforces our assumption and that previously made within [15, 25] that lithium plating is largely reversible within new cells when they are charged.

4.2.2 Adaptive Charge Control

Unlike previous studies which derived the charging strategy off-line [1, 9], both the proposed methods of fast-charge control can be adapted to online use with the ability to adapt their behaviour as the overall degradation of the cell changes. This is because the identification of $V_{HCC\text{-}end}$ is based on the latest battery operation information and requires simply measurements of current and cell terminal voltage. As can be seen from Figure 6d and Figure 9b, $V_{HCC\text{-}end}$ for the plating control strategy reduced when the reversible plating was detected and then increased after the onset of reversible plating was no longer observed. This shows that lithium plating detection-based control has the potential to develop into an adaptive charge control strategy that can adjust the battery charging approach based on the real-time working conditions experienced by the cell. Similarly, the ΔSOH-based control approach relies on the measurement of capacity fade of the current cycle to regulate the $V_{HCC\text{-}end}$ to control the capacity fade rate and therefore can also adapt to the battery ageing within a real-time control application.

4.2.3 Research opportunities, challenges and future work

a) Offline implementation

Both the proposed non-destructive approaches are valuable in devising offline charge profiles to avoid the onset of plating. The research within this paper focuses on a specific case where the charge rate and temperature were set to 1C and 5^{o}C respectively. This same methodology and test procedure can be more generalized to other working conditions to identify the optimal V_{tc} at the end of the first CC stage. For the 2nd stage CC current, a plating sensitivity analysis as described within [30] is necessary to identify the corresponding current at each temperature and fast charge current value. Once the offline characterization is completed, this model can then be used in a real-time application where $V_{HCC\text{-}end}$ is selected according to the operating conditions. This can help avoid large levels of lithium plating in the initial few cycles (as observed in set B cells in this work during the optimization of $V_{HCC\text{-}end}$) and thus, can extend battery life further compared to the performance of set B cells.

Further, to take account of VRP method's insensitivity to low levels of plating (below 2.5% of plating as discussed in [26]), an additional safety margin while selecting the $V_{HCC\text{-}end}$ can be considered to further guarantee the plating free charging event. For example, fast charging can be terminated 25 mV below the identified $V_{HCC\text{-}end}$.

While using the ΔSOH-based method for the development of offline charge profiles, the impact of interruption frequency of capacity tests on the capacity fade rate of fast charging cycles needs to be considered. As discussed within [39], increased interruption of fast charging cycles for capacity tests reduces the capacity fade rate. Therefore, to avoid a significant drop in the SOH level while identifying the V_{tc} at a selected SOH level, the capacity estimation test can be performed after every fast charging cycle. Further, for a fair comparison of different fast charging algorithms, the fast charging tests shall be designed such that all the battery cells in different groups undergo the same frequency of capacity characterization tests. The offline charge profiles will be developed and verified in comparison with the traditional CC-CV and other charge profiles found in the literature [21] as part of our future work.

b) Online implementation

The proposed methods are based on on-board measurable parameters and their rate of change measured in real applications and can be, this way, integrated into a Battery Management System (BMS) for the development of dynamic charge profiles. However, there exist challenges towards the online implementation of these techniques that must be addressed.

For the VRP based method, there are three major challenges that need to be addressed. First, the detection sensitivity of plating can drop as battery ages [31], and thus the VRP method can fail to detect the occurrence of plating. For example, as observed in this work, even after reversible lithium plating becomes undetectable by the VRP method, the capacity fade of cells contained within sets A and B, were observed to continue as explained in section 4.1.5. As a result, the plating detection-based charge control (set B) still experienced higher levels of capacity fade as compared to the ΔSOH-based charge control after plating detection disappeared. As discussed within [40], a reduction of reversible lithium plating and/or its detection sensitivity with battery ageing can result in failure of the plating detection technique to properly identify the onset of lithium plating. The detection sensitivity of reversible lithium plating is highest if charging is terminated as soon as the NEP regains to a positive level [28, 30]. From our previous research [30], the optimal cut-off current in the CV phase of the CC-CV charging profile that produces the highest plating detection sensitivity could be found for a new cell. Since the NEP and its potential drop changes with ageing and charge profile, it is possible that this optimum threshold condition can vary. As a result, the detection sensitivity of the VRP method with a fixed 0.25C cut-off charge rate may reduce and fail to properly detect lithium-plating occurrence as cells age. Further work is therefore required to study the detection sensitivity of the VRP method for different cell ageing levels. In addition, new approaches either through experimentation or modelling may be required to improve the detection sensitivity in such a manner that is transferable to different cell technologies.

Second, since the VRP method depends on the relaxation in post-charge conditions, a further study is necessary to fully understand the usage patterns in real-time that might affect the periods immediately after battery charge. For example, charging the battery in fast charging stations may not allow the cell to undergo the required relaxation. However, the usual end of day charging at home may provide sufficient time to observe the voltages in relaxation. Therefore, a further study is required to combine offline and online charge control strategies based on the charging patterns observed in real-time use.

Third, the temperature changes during the rest period can influence the lithium stripping reaction rate and thus plating detection using the VRP method [40]. With the use of active cooling, the cell surface temperature was maintained constant in this work. However, in practical applications, temperature variations are known to be unavoidable [19]. Therefore, a further study is necessary to better understand the impact of temperature changes on the VRP method capability.

The ΔSOH based charge control strategy can be extended to different types of lithium-ion cells irrespective of their format and chemistries since it is based on a direct measure capacity fade. However, use of such a technique in real-time applications, particularly in EVs is difficult because of the high-accurate current measurement and regular operation of full charge-discharge requirements to estimate the retained capacity within the cell accurately. Future

development of battery research may lead to accurate online battery capacity estimation method that can meet the requirement for the ΔSOH based charging control, but until then, the authors suggest using it offline.

Further, both these techniques that aim to reduce lithium plating may fail to limit the degradation rate if lithium metal depositions from previous lithium plating increase the mechanical stresses within the NE. As explained in [8], the plated lithium occupies nearly four times more volume than intercalated lithium within the electrode. Therefore, this may cause additional loss of active material (LAM) in the electrodes in both cells from sets A and B which experienced plating. Previous work [15] assumes that lithium plating caused only a loss of lithium inventory (LLI) while LAM rate was assumed to be constant over cycle number. However, as discussed in [8] and evidenced by the continued capacity losses even after lithium plating becomes undetectable in Set A and Set B cells, there is a possibility of increased mechanical stresses during and after charge cycles where lithium plating has occurred. Therefore, a further study is necessary to better understand the limitations of the charging control strategies within cells that have experienced lithium plating at some point during their operational life by quantifying the degradation modes using differential voltage (DV) curves [15, 41]. Further, DV analysis along with an assessment of Coulombic efficiency [4] may help to understand whether plating becomes increasingly irreversible as the battery ages. For example, capacity imbalances between the electrodes and lithiation level of the NE at the end of charge may indicate the occurrence of lithium plating [15]. Reduced Coulombic efficiency and non-detection of reversible plating under potential plating conditions may highlight large levels of irreversible plating.

5. Conclusions

From the experimental results obtained for a commercially available NCA cell at 5^{o}C and 1C charge rate, significant lithium plating was observed within all cells when they were charged using a traditional CC-CV charge protocol. Accordingly, the cells were found to have lost 20% of their nominal capacity over the 52 fast charge cycles. A simple reduction of $V_{HCC\text{-}end}$ from the V_f can reduce lithium plating, which, however, will prolong the charging time. To minimize the impact of the modified charge profile on the charging time while concurrently avoiding lithium plating, two advanced non-destructive charge control approaches have been introduced. In the first approach, the VRP-method of lithium-plating detection is used to improve charge performance. The cell terminal voltage V_{tc} is identified where the NEP reduces below the Li\Li^{+} reference and defines the condition for lithium plating to occur. Unlike previous research, this approach enabled the identification of V_{tc} directly on commercial cells without modifications being required. This potentially makes the technique more suitable for practical implementation. The second method studied how a measure of overall battery capacity reduction per cycle, ΔSOH, can be used to define the transition point between CC and CV charge stages to minimise battery degradation. Both techniques are employed with a new CC-CV-CC charge profile. Experimental results highlight that the capacity fade of cells using the proposed charging strategies can be significantly reduced compared to when charged using the conventional CC-CV approach by 45 and 70% respectively while minimizing their impact on the charging speed. Further work involves embedding the lithium plating identification technique within a real-world battery charge application, such as within an EV, to better quantify the benefits associated with its use. In particular, its ability to simultaneously reduce charge time and extend battery life and to better address the research challenges associated with adapting the critical voltage (V_{tc}) to take account of subtle variations in cell characteristics and behaviour as the technique is used on different cell technologies.

References

1. Anseán, D., et al., *Fast charging technique for high power lithium iron phosphate batteries: A cycle life analysis.* Journal of Power Sources, 2013. **239**: p. 9-15.
2. Guo, Z., et al., *Optimal charging method for lithium ion batteries using a universal voltage protocol accommodating aging.* Journal of Power Sources, 2015. **274**: p. 957-964.
3. Waldmann, T., et al., *Temperature dependent ageing mechanisms in Lithium-ion batteries – A Post-Mortem study.* Journal of Power Sources, 2014. **262**: p. 129-135.
4. Downie, L.E., et al., *In Situ Detection of Lithium Plating on Graphite Electrodes by Electrochemical Calorimetry.* Journal of the Electrochemical Society, 2013. **160**(4): p. A588-A594.
5. Ren, D., et al., *Investigation of Lithium Plating-Stripping Process in Li-Ion Batteries at Low Temperature Using an Electrochemical Model.* Journal of The E lectrochemical Society, 2018. **165 (10) A2167-A2178**
6. Uhlmann, C., et al., *In situ detection of lithium metal plating on graphite in experimental cells.* Journal of Power Sources, 2015. **279**: p. 428-438.
7. Waldmann, T., et al., *Interplay of Operational Parameters on Lithium Deposition in Lithium-Ion Cells: Systematic Measurements with Reconstructed 3-Electrode Pouch Full Cells.* Journal of The Electrochemical Society, 2016. **163**(7): p. A1232-A1238.
8. Bitzer, B. and A. Gruhle, *A new method for detecting lithium plating by measuring the cell thickness.* Journal of Power Sources, 2014. **262**: p. 297-302.
9. Waldmann, T., M. Kasper, and M. Wohlfahrt-Mehrens, *Optimization of Charging Strategy by Prevention of Lithium Deposition on Anodes in high-energy Lithium-ion Batteries – Electrochemical Experiments.* Electrochimica Acta, 2015. **178**: p. 525-532.
10. Ye, Y., et al., *Simulation and evaluation of capacity recovery methods for spiral-wound lithium ion batteries.* Journal of Power Sources, 2013. **243**: p. 779-789.
11. Moura, S.J., et al., *Battery State Estimation for a Single Particle Model With Electrolyte Dynamics.* IEEE Transactions on Control Systems Technology 2017. **Volume: 25 , Issue: 2**.
12. Lewerenz, M., A. Warnecke, and D.U. Sauer, *Post-mortem analysis on LiFePO 4 |Graphite cells describing the evolution & composition of covering layer on anode and their impact on cell performance.* Journal of Power Sources, 2017. **369**: p. 122-132.
13. Eckera, M., P.S. Sabeta, and D.U. Sauer, *Influence of operational condition on lithium plating for commercial lithium-ion batteries – Electrochemical experiments and post-mortemanalysis.* Applied Energy. **206**: p. 934-946.
14. Klett, M., et al., *Non-uniform aging of cycled commercial LiFePO4//graphite cylindrical cells revealed by post-mortem analysis.* Journal of Power Sources, 2014. **257**: p. 126-137.
15. Anseán, D., et al., *Operando lithium plating quantification and early detection of a commercial LiFePO 4 cell cycled under dynamic driving schedule.* Journal of Power Sources, 2017. **356**: p. 36-46.
16. Frisco, S., et al., *Understanding Li-Ion Battery Anode Degradation and Pore Morphological Changes through Nano-Resolution X-ray Computed Tomography.* Journal of The Electrochemical Society, 2016. **163**(13): p. A2636-A2640.
17. Liu, Y.-H., C.-H. Hsieh, and Y.-F. Luo, *Search for an Optimal Five-Step Charging Pattern for Li-Ion Batteries Using Consecutive Orthogonal Arrays.* IEEE Transactions on Energy Conversion, 2011. **26**(2): p. 654-661.
18. Savoye, F., et al., *Impact of Periodic Current Pulses on Li-Ion Battery Performance.* IEEE Transactions on Industrial Electronics, 2012. **59**(9): p. 3481-3488.
19. Zhang, C., et al., *Charging optimization in lithium-ion batteries based on temperature rise and charge time.* Applied Energy, 2017. **194**: p. 569-577.
20. Perez, H.E., et al., *Optimal Charging of Li-Ion Batteries With Coupled Electro-Thermal-Aging Dynamics.* IEEE Transactions on Vehicular Technology, 2017. **66**(9): p. 7761-7770.
21. Keil, P. and A. Jossen, *Charging protocols for lithium-ion batteries and their impact on cycle life—An experimental study with different 18650 high-power cells.* Journal of Energy Storage, 2016. **6**: p. 125-141.

22. Bach, T.C., et al., *Nonlinear aging of cylindrical lithium-ion cells linked to heterogeneous compression.* Journal of Energy Storage, 2016. **5**: p. 212-223.
23. Ge, H., et al., *Investigating Lithium Plating in Lithium-Ion Batteries at Low Temperatures Using Electrochemical Model with NMR Assisted Parameterization.* Journal of The Electrochemical Society, 2017. **164**(6): p. A1050-A1060.
24. Lewandowski, A., A. Swiderska-Mocek, and L. Waliszewski, *Solid electrolyte interphase formation on metallic lithium.* J Solid State Electrochem, 2012. **16:3391–3397**.
25. Smart, B.V.R.a.M.C., *Lithium Plating Behavior in Lithium-ion Cells.* ECS Transactions, 25 (36) 241-252 (2010).
26. von Lüders, C., et al., *Lithium plating in lithium-ion batteries investigated by voltage relaxation and in situ neutron diffraction.* Journal of Power Sources, 2017. **342**: p. 17-23.
27. Schindler, S., et al., *Voltage relaxation and impedance spectroscopy as in-operando methods for the detection of lithium plating on graphitic anodes in commercial lithium-ion cells.* Journal of Power Sources, 2016. **304**: p. 170-180.
28. Petzl, M. and M.A. Danzer, *Nondestructive detection, characterization, and quantification of lithium plating in commercial lithium-ion batteries.* Journal of Power Sources, 2014. **254**: p. 80-87.
29. Schuster, S.F., et al., *Nonlinear aging characteristics of lithium-ion cells under different operational conditions.* Journal of Energy Storage, 2015. **1**: p. 44-53.
30. Koleti, U.R., et al., *A new concept to improve the lithium plating detection sensitivity in lithium-ion batteries.* International Journal of Smart grid and Clean Energy, 2019. **Accepted for publication**.
31. Zinth, V., et al., *Lithium plating in lithium-ion batteries at sub-ambient temperatures investigated by in situ neutron diffraction.* Journal of Power Sources, 2014. **271**: p. 152-159.
32. Yang, X.-G., et al., *Modeling of lithium plating induced aging of lithium-ion batteries: Transition from linear to nonlinear aging.* Journal of Power Sources, 2017. **360**: p. 28-40.
33. Troxler, Y., et al., *The effect of thermal gradients on the performance of lithium-ion batteries.* Journal of Power Sources, 2014. **247**: p. 1018-1025.
34. Arora, P., *Capacity Fade Mechanisms and Side Reactions in Lithium-Ion Batteries.* Journal of The Electrochemical Society, 1998. **145**(10): p. 3647.
35. Lewerenz, M., A. Warnecke, and D.U. Sauer, *Introduction of capacity difference analysis (CDA) for analyzing lateral lithium-ion flow to determine the state of covering layer evolution.* Journal of Power Sources. **354**: p. 157-166.
36. Lewerenz, M., et al., *Irreversible calendar aging and quantification of the reversible capacity loss caused by anode overhang.* Journal of Energy Storage, 2018. **18**: p. 149-159.
37. Lewerenz, M., et al., *Systematic aging of commercial LiFePO 4 |Graphite cylindrical cells including a theory explaining rise of capacity during aging.* Journal of Power Sources, 2017. **345**: p. 254-263.
38. Schmalstieg, J., et al., *A holistic aging model for Li(NiMnCo)O2 based 18650 lithium-ion batteries.* Journal of Power Sources, 2014. **257**: p. 325-334.
39. Lewerenz, M., P. Dechent, and D.U. Sauer, *Investigation of capacity recovery during rest period at different states-of-charge after cycle life test for prismatic Li(Ni1/3Mn1/3Co1/3)O2-graphite cells.* Journal of Energy Storage, 2019. **21**: p. 680-690.
40. Yang, X.-G., et al., *A look into the voltage plateau signal for detection and quantification oflithium plating in lithium-ion cells.* Journal of Power Sources, 2018. **395**: p. 251-261.
41. Birkl, C.R., et al., *Degradation diagnostics for lithium ion cells.* Journal of Power Sources, 2017. **341**: p. 373-386.